Applied Catalysis B: Environmental 220 (2018) 367–378

Contents lists available at ScienceDirect

Applied Catalysis B: Environmental

journal homepage: www.elsevier.com/locate/apcatb

Research Paper

Fabrication of nanostructured flowerlike p-BiOI/p-NiO heterostructure and its efficient photocatalytic performance in water treatment under visible-light irradiation

Leila Yosefi [a,b], Mohammad Haghighi [a,b,*]

[a] Chemical Engineering Faculty, Sahand University of Technology, P.O. Box 51335-1996, Sahand New Town, Tabriz, Iran
[b] Reactor and Catalysis Research Center (RCRC), Sahand University of Technology, P.O. Box 51335-1996, Sahand New Town, Tabriz, Iran

ARTICLE INFO

Article history:
Received 20 April 2017
Received in revised form 10 July 2017
Accepted 7 August 2017
Available online 9 August 2017

Keywords:
p-p BiOI/NiO heterostructures
Precipitation
Solvothermal
Nanophotocatalyst
Water treatment

ABSTRACT

Bismuth-related nanomaterials have received intense attention as potential promising photocatalysts for environment remediation. BiOI is well-known due to efficient photocatalytic activity, high stability, low cost and nontoxicity. In this study, novel nanostructured high-yield visible-light-induced photocatalyst p-BiOI/p-NiO was synthesized by a facile solvothermal method. Several characterization methods, such as X-ray powder diffraction (XRD), scanning electron microscopy (SEM), Energy dispersive X-ray analysis (EDX), Fourier Transform Infrared Spectroscopy (FTIR), the Brunauer–Emmett–Teller (BET) surface area, photoluminescence (PL) spectroscopy and UV–vis diffuse reflectance spectroscopy (DRS) were employed to study the phase structures, morphologies and optical properties of the samples. The photocatalytic properties of the as-prepared products were measured with the degradation of acid orange 7 (AO7) at room temperature under visible light illumination. It was found that the NiO amount in the BiOI/NiO composites played an important role in the corresponding photocatalytic properties. The best performance was achieved at 10% content. Enhanced photocatalytic activity of the composites was due to the improved photogenerated carrier separation capacity due to suitable heterojunction formation. In addition the mechanism was proposed for the coupled semiconductors. The reusability of nanophotocatalyst and effects of pH, dye concentration and photocatalyst dosage were also investigated.

1. Introduction

Nowadays, visible-light-driven photocatalyst has been proved to be a promising technology for diversity of applications such as energy field and elimination of environmental contaminants [1–3]. Large quantity of synthetic dyes discharged into the aquatic environment through their synthesis and application in textile, cosmetic and leather processing industries. Most importantly their variety, toxicity and resistance endanger the human beings, aquatic and land life by contamination of water supply [4–7]. Thus their elimination is a vital environmental issue [8]. Among large amounts of organic and synthetic dyes, Azo dyes are bio-recalcitrant, likewise coagulation and adsorption purification methods cause secondary pollution [9,10]. Photocatalysis is well-known as a green approach for water and air purification because of solar energy utilization as an unlimited, inexpensive and environmentally friendly energy resource [11–13]. Although conventional semiconductor photocatalysis such as TiO_2, ZnO are cost-effective, non-toxic, they have wide band gap (~3.2 eV) and actually are UV absorber which consist only 4% of solar light irradiation which is one of their practical application hindrances [14–16]. Therefore extensive efforts on exploiting novel semiconductor materials with narrow band gap, visible-light active with high quantum efficiency are highly desired. Bi oxyhalides due to high stability, low cost, nontoxicity and remarkable visible-light photocatalytic activity have received many attentions [17–19]. They are constructed from $[Bi_2O_2]^{+2}$ slabs intercalated with halogen atoms. This unique layered structure forms an internal electric field which improves photo-induced charge carrier generation and separation [20]. Among them BiOI has narrowest band gap (1.7–1.9 eV) and strongest ability of harvesting visible light irradiation [21–23]. However individual application of BiOI is restricted by fast recombination rate of photo-generated electron-hole pairs. Undoubtedly one of effective structures for enhancement of BiOI photocatalytic activity is coupling with a wide band gap semiconductor [24–26].

* Corresponding author. Reactor and Catalysis Research Center, Sahand University of Technology, P.O. Box 51335–1996, Sahand New Town, Tabriz, Iran.
E-mail address: haghighi@sut.ac.ir (M. Haghighi).

http://dx.doi.org/10.1016/j.apcatb.2017.08.028
0926-3373/

As a matter of fact semiconductor-semiconductor heterojunction is an efficacious architecture for separation of photo-excited electron hole pairs. In non-*p*-*n* heterojunction systems the two semiconductors are tightly staggered together [27]. In this case VB and CB of one semiconductor settle lower than the VB and CB of the other one. Electrons from higher CB level transfer to the lower one and the holes transfer to the VB of semiconductor with higher level [28,29]. Consequently generation and separation of charge carriers are effectively provided. While internal electric field is improved, recombination will be largely reduced andw[30–34]. A considerable number of electrons on the CB of semiconductor A and large number of holes on the VB of semiconductor B take part in photodegradation process [35–38]. Thus photocatalytic activity will be highly improved. BiOI mostly coupled with an n-type wide band gap semiconductors due to its small band gap [39–41]. Several works have been reported in this issue such as BiOI/Zn_2SnO_4 [42], BiOI/Bi_2WO_6 [43], BiOI/TiO_2 [44], BiOI/Bi_2O_3 [45] and etc have been proved to be effective. While few reports have been performed about p-p type heterojunction of bismuth oxyhalides except BiOX family combinations. NiO is a stable p-type semiconductor having rock salt structure with wide variety of applications in gas sensors, catalysis, adsorbents, solar cells, electrochemical supercapacitors, sensors, lithium ion batteries and so on [46–50]. NiO nanoparticles have been widely used because of stability, excellent chemical, physical, electronic and magnetic properties [15,30,31]. Furthermore NiO has been used as adsorbent for toxic Cr(VI) removal from water, acid red, cango red and other organic dyes or heavy metals [51]. Till now several works about NiO heterojunctions have been reported such as NiO/TiO_2 [52], NiO/Fe_2O_3 [53], NiO/ZnO [54], NiO/CdS [55], NiO/C_3N_4 [56]. NiO individually hasn't photoactivity, but can be sensitised by BiOI as notable visible light absorber. On the other hand, NiO will inhibit recombination of photo-induced charge carriers in BiOI. NiO nanoparticles have been prepared by different methods such as sol-gel, solvothermal, precipitation, microemulsion, hydrothermal and so on. Among different synthesis methods, it is important to be prepared synthesize by facile, cost effective, simple equipment and repeatable method Hence [49,57–60]. To this aim precipitation method is selected for synthesis of NiO nanoparticles. To the best of our knowledge synthesis and characterization of BiOI/NiOI nanophotocatalyst and it photocatalytic activity in comparison with pure BiOI and NiO has not been reported to date.

Herein, we reported a novel p-BiOI/p-NiO composite synthesized by facile solvothermal method over precipitated NiO. Its photoactivity is investigated for AO7 removal from water under visible light irradiation. Moreover, a photocatalytic mechanism was proposed based on the relative band position of these two semiconductors. Chemical, physical and optical properties of prepared samples are investigated by (XRD), (FESEM), (EDX Dot-Mapping), (BET), (FTIR), (PL) and (DRS). Finally, photocatalytic activity test was carried out and parameters such as initial pH, photocatalyst loading and AO7 concentration were investigated.

2. Materials and methods

2.1. Materials

Different reagents have been used in this work: Ni(NO3)3.6H2O as NiO precursor and NaOH was used as precipitating agent. Bi(NO3)3.5H2O, KI as precursors for BiOI, were purchased from Merck company. Ethanol and AO7(acid orange 7) as a representative of dye pollutants also was purchased from Merck company.

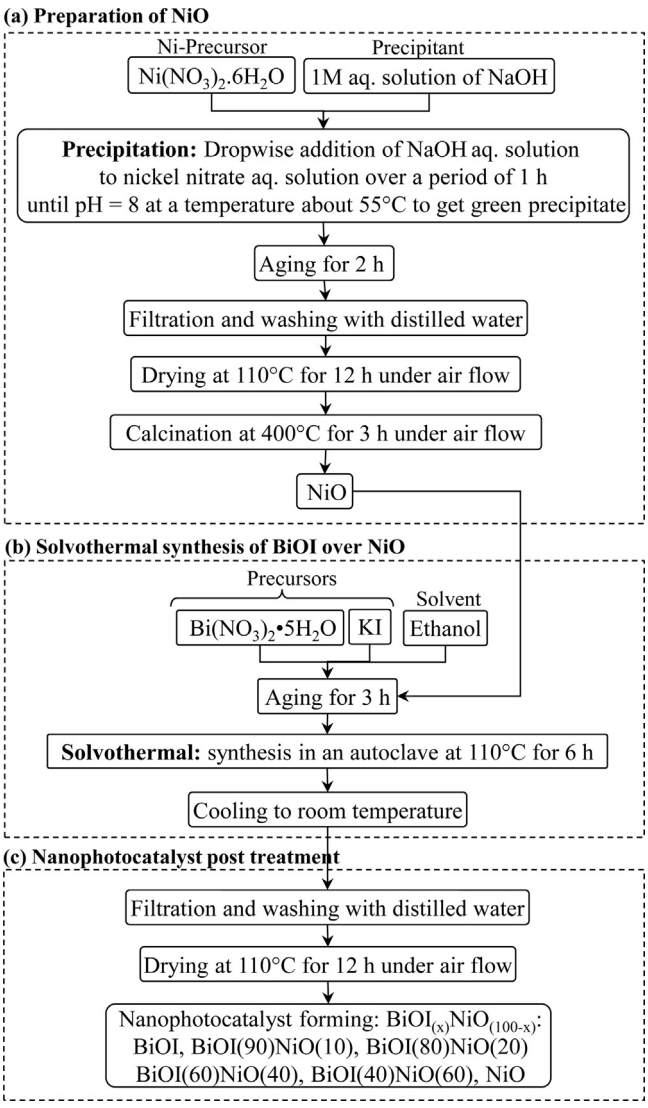

Fig. 1. Precipitation dispersion of NiO over solvothermal synthesized flowerlike BiOI nanostructure as an enhanced visible light nanophotocatalyst.

2.2. Nanostructured photocatalysts preparation and procedure

As illustrated in Fig. 1 in the first step, NiO was synthesized by a precipitation route. Analytical pure $Ni(NO_3)_2{\cdot}6H_2O$ reagents was dissolved in deionized water. $Ni(OH)_2$ was precipitated by dropwise addition of 1 M NaOH aqueous solution until the pH reached to 8. After 2 h aging at 55 °C the green precipitant was washed with deionized water for several times. Subsequently, the slurry was filtered and dried at 110 °C for 12 h under air flow. Then the sample was calcined at 400 °C for 3 h.

Secondly, nano-structured BiOI/NiO with different loadings 90/10, 80/20, 60/40, 40/60 were prepared using a simple solvothermal method. Bi(NO3)3.5H2O, KI, and as-prepared NiO were dissolved in 100 mL ethanol. After mixing under vigorous stirring for 3 h the suspension was transfer to a 150 mL Teflon-lined stainless steel autoclave and maintained at 100 °C for 6 h. The autoclave was cooled to room temperature naturally. Then the resulted dark red precipitate was filtered and washed several times with distilled water and ethanol, Afterward dried at 110 °C for 12 h.

2.3. Nanostructured photocatalysts characterization techniques

In this research the phase composition of synthesized samples were characterized by an X-Ray diffractometer (XRD Siemens D5000) equipped with Ca Kα X-Ray source (2θ ranging from (10° to 80°). The field emission scanning electron microscopy (FESEM, HITACHI S$109 4160) analyser employed to observe the morphologies and structure of synthesized nanophotocatalysts. Energy dispersive X-ray analysis used for elemental analysis and dispersion of elements was performed by EDX-dot mapping analysis (VEGA\\TESCAN, BSE detector). Specific surface area of powders was characterized by N_2 adsorption and desorption isotherms obtained at 196 °C using a Quantachrome CHEMBET 3000 unit applying the standard Brunauer, Emmett and Teller (BET) method. Fourier Transform Infrared Spectroscopy (FTIR, UNICAM 4600) was employed in the range of 400–4000 cm^{-1} wave number K-Br pellet method for observation of surface functional groups. UV–vis (DRS) was recorded in air atmosphere at room temperature in a wavelength range of 200–800 nm using a (Scinco S4100 spectrophotometer). The photoluminescence (PL) spectroscopy, obtained at room temperature with anexcitation wavelength of 320 nm, were recorded on a Perkin Elmer (USA) fluorescence spectrophotometer.

2.4. Experimental setup for photocatalytic performance test

The photocatalytic activity of the nanostructured photocatalysts was carried out by the degradation of AO7 aqueous solution under visible light illumination. To this aim, the 20 mg/L AO7 was mixed with 100 mL of solution filled with 0.1 g photocatalyst. Before irradiation, the suspension was stirred in a Pyrex photoreactor in a dark place for 1 h to establish adsorption–desorption equilibrium between dye molecules and photocatalysts. The 400 W halogen lamp (OSRAM, Germany) was applied to provide visible light irradiation focused on the photoreactor. The 0 °C water bath and cooling air was used to maintain Pyrex tube reactor temperature in 25 °C. Irradiation starts at time t = 30 min and at certain time intervals 5 mL suspension was taken. The residual concentration of AO7 in the solution was measured at a maximum wavelength of 485 nm by UV–vis spectrophotometer. The degradation efficiency percent was calculated by the following Eq. (1)

$$\text{DegradationEfficiency}(\%) = (1 - C/C0) * 100 \quad (1)$$

C0 is initial concentration of the AO7 after dark and C is final concentration in the solution, respectively.

3. Results and discussions

3.1. Nanostructured photocatalysts characterization

3.1.1. XRD analysis

In order to investigate crystalline phase of nano-photocatalysts XRD analysis is applied. Fig. 2 represents XRD patterns of BiOI, BiOI(90)/NiOI(10), BiOI(80)/NiOI(20), BiOI(60)/NiOI(40), BiOI(40)/NiOI(60) and NiOI. The results show that the as-synthesized samples were well crystallized and all the diffraction peaks of BiOI were in one tetragonal phase coincided with the standard JCPDS file of BiOI (No. 01-073-2062). As it can be seen all diffraction peaks indexed to BiOI can be seen in 19.3°, 29.7°, 31.7°, 37.2°, 37.5°, 39.5°, 43.8°, 45.8°, 51.5°, 55.3°, 60.4°, 66.5°, 74.3°, 75.4°, 88.6°. The intense peaks at 29.7°, 31.7°, 45.8° and 55.3° indexed to (012), (110), (020) and (122) planes respectively. It is obvious diffraction peaks intensities of BiOI weakened while NiO content increased. The diffraction peaks of NiO are in accordance with JCPDS No. 01-073-1519 with cubic phase. No other characteristic peaks rather than what expected is detected. Indicating the composites are made from pure materials and no other phases are created during synthesis of each component.

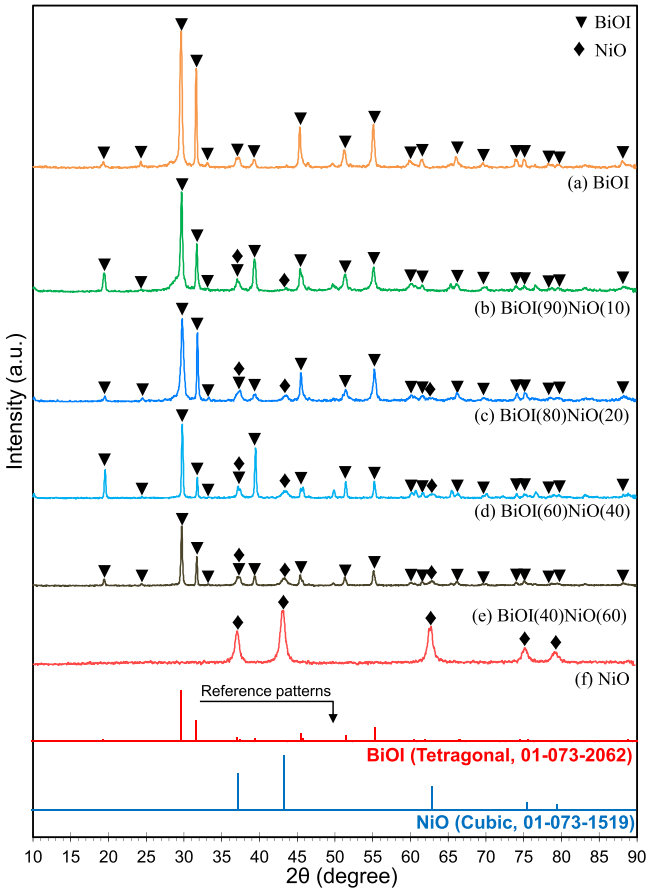

Fig. 2. XRD patterns of BiOI(x)-NiO(100-x) nanophotocatalysts: (a) BiOI, (b) BiOI(90)NiO(10), (c) BiOI(80)NiO(20), (d) BiOI(60)NiO(40), (e) BiOI(40)NiO(60)and (f) NiO.

3.1.2. FESEM analysis

Fig. 3 depicts FESEM images of as-prepared samples. Pure BiOI consists from thin flakes with thickness of 24.2 nm. These thin nanoflakes assembled together and constructed microflowers with average diameter of 2 μm (Fig. 3a). After NiO modification, NiO nanoparticles randomly dispersed on the surface of BiOI nanosheeets. In the BiOI(90)/NiO(10), BiOI(20)/NiOI(80) and BiOI(60)/NiO(40) samples NiO nanoparticles can be seen on the surface of BiOI nanosheets. Appropriate dispersion of NiO nanoparticles provides effective physical junction between two semiconductors that undoubtedly will improve generation and separation of photo-induced electron-hole pairs due to p-p type heterostructures of composite. It can be seen that by increasing NiO content the morphology of BiOI clearly changed and the flower-like structures with smaller sheets are constructed. By increasing NiOI content up to 40% the main structure of BiOI is preserved and nanoparticles of NiO covered the BiOI plates uniformly (Fig. 3d). On the other hand by 60 percent of NiO loading the structure of BiOI is hidden and only NiO nanoparticles are observable. It can be conclude that NiO nanoparticle thoroughly covered the surface of BiOI nanosheets. NiO nanoparticles synthesized from simple precipitation method possess homogenous nanoparticles with average particle size of 12.6 nm.

Fig. 4 depicts particle size distribution histogram of BiOI(90)/NiO(10) and NiO samples. As it is clear the nanoparticles distribution was in nanoscale and mainly are in the range of

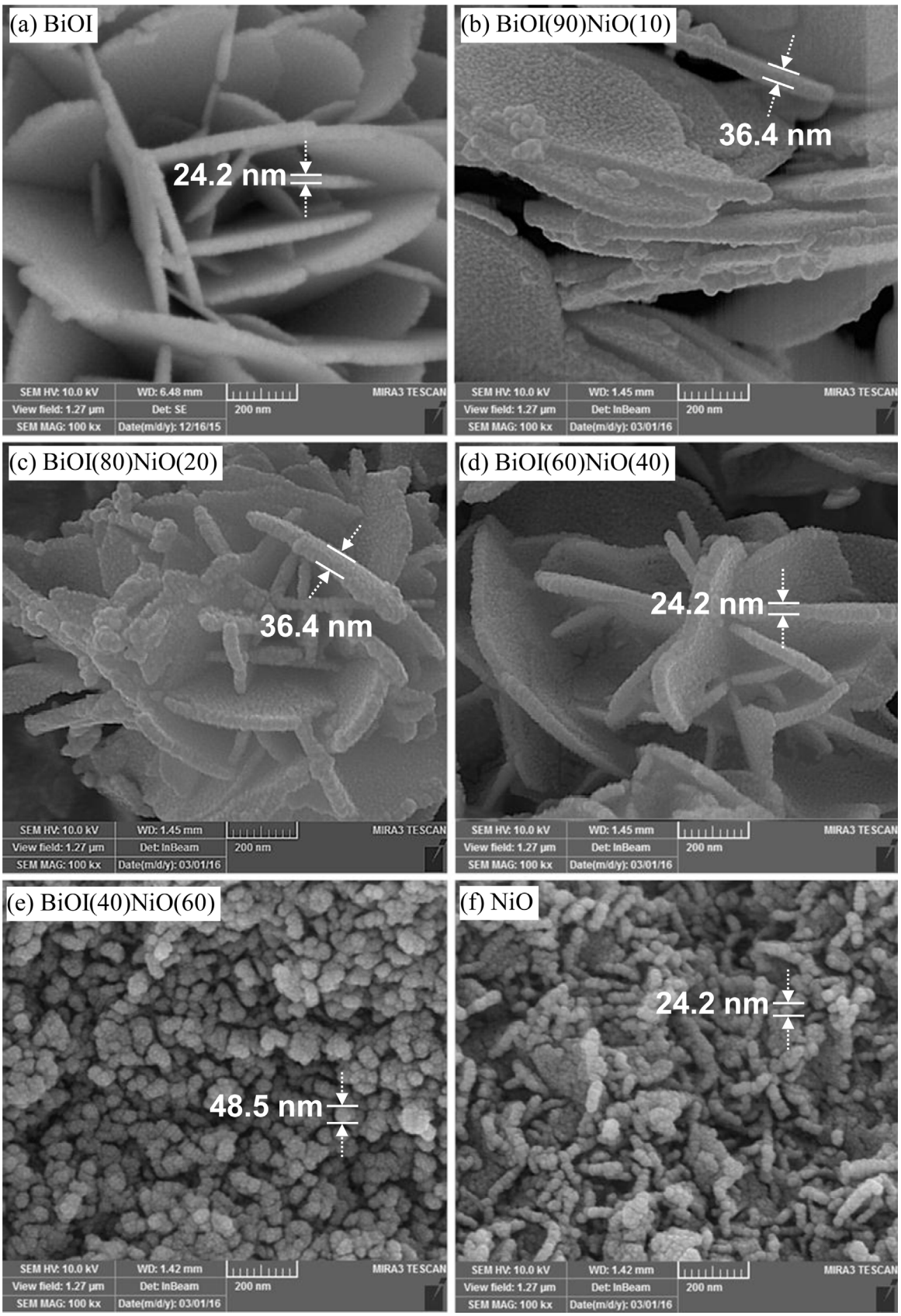

Fig. 3. FESEM images of BiOI(x)-NiO(100-x) nanophotocatalysts: (a) BiOI, (b) BiOI(90)NiO(10), (c) BiOI(80)NiO(20), (d) BiOI(60)NiO(40), (e) BiOI(40)NiO(60)and (f) NiO.

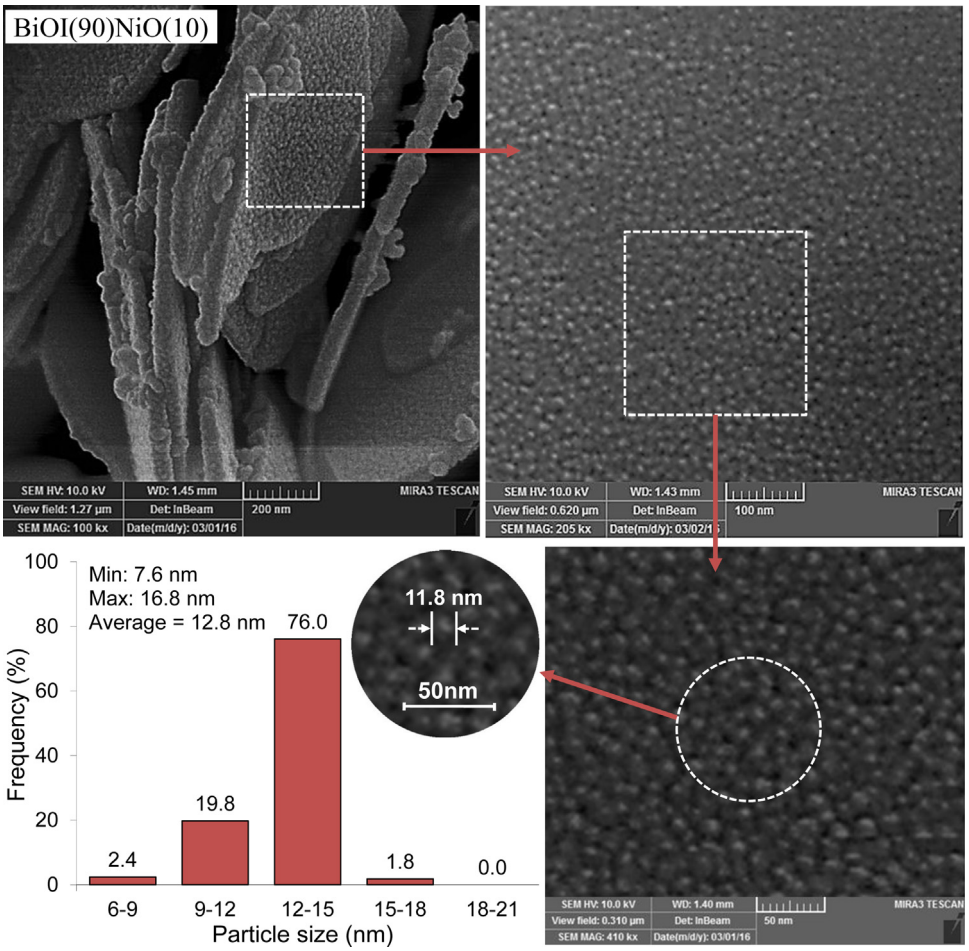

Fig. 4. Surface particle size histogram of BiOI(x)-NiO(100-x) nanophotocatalyst: BiOI(90)NiO(10). 30.

12–15 nm. More over 76.0% of the particle size have the average size of 12.8 nm. The maximum and minimum of naoparticles are 7.6 nm and 16.8 nm respectively. It is worth to note that NiO nanoparticle will make greater tight coupling than bulk NiO which is well prepared in the as-synthesized sample.

3.1.3. EDX analysis

Fig. 5 illustrates EDX analysis of BiOI, BiOI(90)/NiO(10), BiOI(80)/NiO(20), BiOI(70)/NiO(30), BiOI(60)/NiO(40), and NiO samples. The result of elemental analysis of gold coated samples shows independent peaks for Bismuth (Bi), Oxygen (O), Iodine (I), Nickel (Ni) which was referring to existence of BiOI and NiO in the as-prepared samples, which are detected in XRD. In order to investigate elements dispersion, EDX dot-mapping micrographs was shown in Fig. 5. It is clear that BiOI(90)/NiO(10) possesses high distribution of Bi, O, I, Ni elements. Noteworthy to say that better distribution provides strong physical coupling in the heterojunction. This provides efficient generation and separation of charge carriers which leads to superior photocatalytic performance of composite. In addition EDX doesn't show any impurity peak which was verified by XRD analysis formerly.

3.1.4. BET analysis

Photocatalytic heterogeneous reactions can be affected by Specific surface area. In order to investigate the effect of this factor in the current study BET analysis was performed. The Brunauer-Emmett-Teller (BET) equation was used to calculate specific surface area and the outcome is illustrated in Fig. 6. The BET surface area of BiOI, BiOI(90)/NiO(10), BiOI(80)/NiO(20), BiOI(60)/NiO(40), BiOI(60)/NiO(40) and NiO was determined to be 10.4, 25.7, 29.7, 21.9, 20.7 and 53 m^2/g, respectively. It can be seen that BiOI has an small specific surface area of $10 m^2/g$. Augmenting NiO content in BiOI/NiO composites, with high specific surface of 53 m^2/g increased BET surface area of BiOI(90)/NiO(10) to 25.7 m^2/g. Further loadings did not cause significant increment in surface area of synthesized composites.

3.1.5. FTIR analysis

Fig. 7 represents FTIR of BiOI, BiOI(90)/NiO(10), BiOI(80)/NiO(20), BiOI(60)/NiO(40), BiOI(40)/NiO(60), NiO. It can be noticed from the figure, at almost all samples adsorption bands of 3500, 2350, and 1640 cm^{-1} were observed, which are attributed to water molecule and hydroxyl group. These vibrations indicate physically adsorbed water in all samples after nanocatalyst heat treatment [61–63]. The sharp peak in NiO sample at 570 cm^{-1} was observed. It can be seen that NiO peak at other composites is decreased as amount of NiO decreased [64,65]. The characteristic peaks of BiOI are verified by the band at 500 and 572 cm^{-1} which refer to stretching vibration of Bi-O [22,26]. Nevertheless, the —OH peak is varied in the samples. The difference observed in the bands intensity is due to physically absorbed water during the mixing and pelleting with KBr by heat treated nanophotocatalysts.

3.1.6. DRS analysis

Fig. 8 displays DRS of the as prepared samples. UV–visible diffuse reflectance spectroscopy is one of the important methods to reveal the energy structures and optical properties of semiconductor nanocrystals. The strongest absorption peak of NiO at

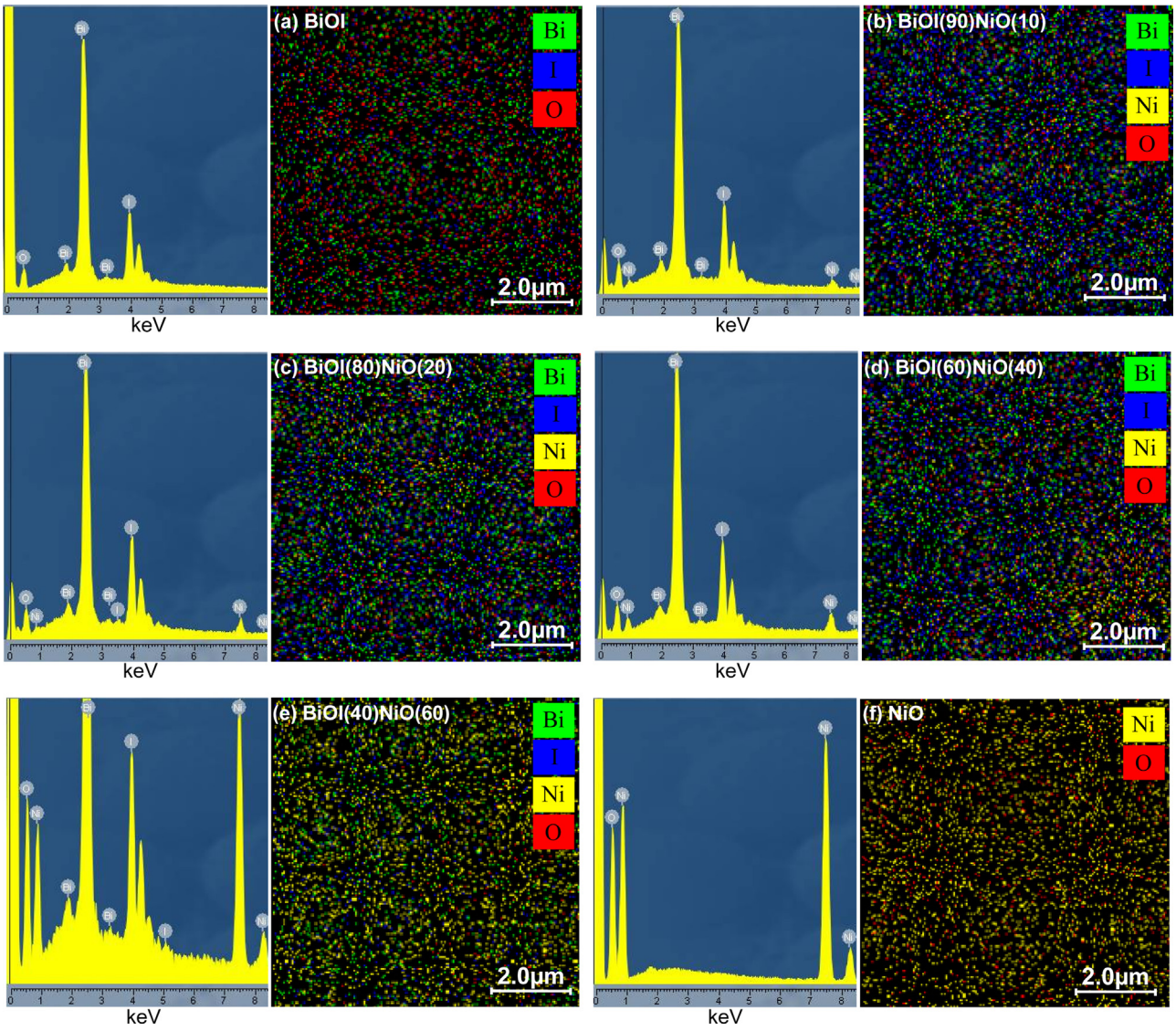

Fig. 5. EDX analysis of BiOI(x)-NiO(100-x) nanophotocatalysts: (a) BiOI, (b) BiOI(90)NiO(10), (c) BiOI(80)NiO(20), (d) BiOI(60)NiO(40), (e) BiOI(40)NiO(60)and (f) NiO.

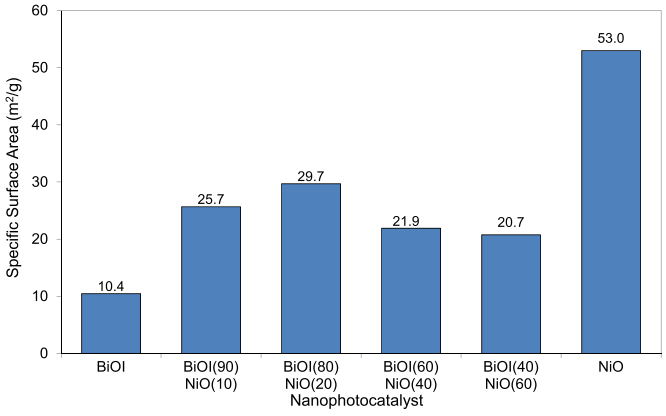

Fig. 6. BET specific surface area of BiOI(x)-NiO(100-x) nanophotocatalysts: BiOI, BiOI(90)NiO(10), BiOI(80)NiO(20), BiOI(60)NiO(40), BiOI(40)NiO(60) and NiO.

wavelength of 313.3 was revealed, which can be attributed to the intrinsic band-gap absorption of NiO due to the electron transitions from the valence band to the conduction band. It is highly approved that quantum size effect, chemical defects or vacancies present in the crystal structure reduce the band gap energy due to generation of new energy levels. It is reported that, as crystallite size of the nanoparticles increases, the energy band gap of the semiconductor decreases [65,66]. It can be observed that absorption edge of BiOI expanded nearly to the whole spectra of visible light. BiOI exhibits absorption edge in the visible light region. It is well known that the optical absorption near the band edge of a crystalline semiconductor can be calculated by the following formula:

$$ah\nu = A(h\nu - Eg)^{n/2} \quad (2)$$

where a, A, ν, h and Eg are the absorption coefficient, a parameter that depend on the interband transition probability, light frequency, Planck constant and band-gap energy, respectively. Among them, n is the number characterizing the nature of the transition process in the semiconductor (direct transition: n = 1; indirect transition: n = 4). For pure BiOI, the value of n is 4 [67], and for pure NiO, the value of n is 1 [65]. The band-gap energy (Eg value) of pure BiOI sample can be thus estimated from a plot of $(ah\nu)^{1/2}$ versus photon energy ($h\nu$), as shown in Fig. 8b, and the band-gap energy (Eg value) of NiO estimated from a plot of $(ah\nu)^2$ versus photon energy as shown in Fig. 8c. The band gap values for BiOI and NiO were estimated to be 1.86 and 3.5 eV, respectively.

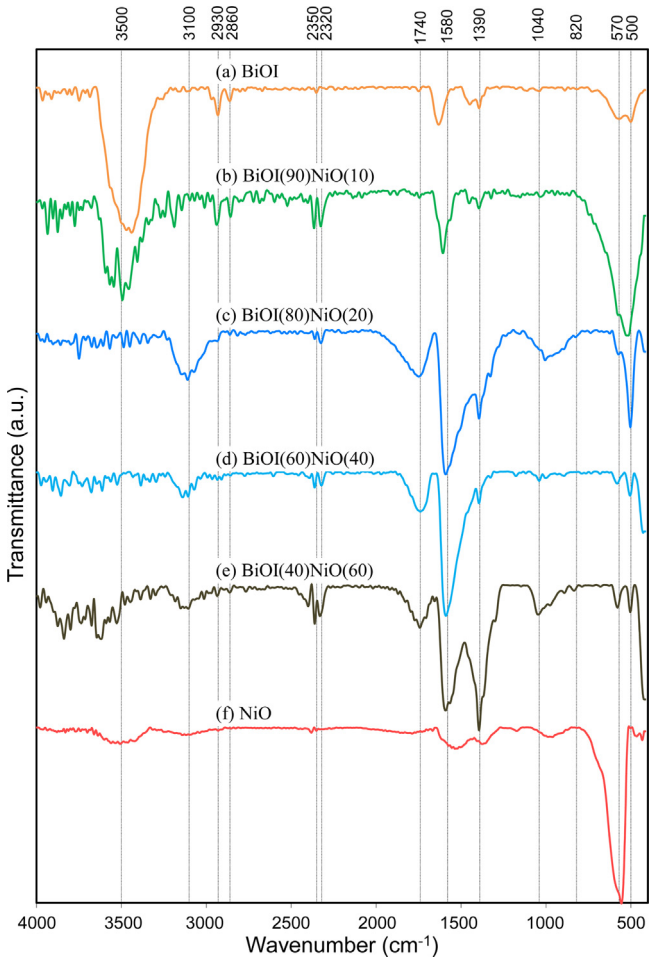

Fig. 7. FTIR spectra of BiOI(x)-NiO(100-x) nanophotocatalysts: (a) BiOI, (b) BiOI(90)NiO(10), (c) BiOI(80)NiO(20), (d) BiOI(60)NiO(40), (e) BiOI(40)NiO(60)and (f) NiO.

3.1.7. Photoluminescence analysis

In order to further investigate the separation efficacy of new heterostructure, PL analysis has been done. Generally photoluminescence spectra originate from recombination of free carriers. Thus it will be an effective tool to survey the separation performance of charge carriers in the composites. Fig. 9 illustrates the PL results for Pure BiOI, NiO and p-BiOI(90)/p-NiO(10) samples. As a matter of fact, the lower PL intensity implies lower recombination of charge carriers. Comparison of PL spectra of samples (excited at 320 nm) displays that p-BiOI(90)/p-NiO(10) with the highest photocatalytic performance possesses the lowest relative PL intensity. Indicating that separation of charge carries is greatly provided through p-BiOI/p-NiO heterostructures.

3.2. Photocatalytic performance study toward acid orange removal from water

3.2.1. Effect of photocatalyst

Adsorption experiments were conducted before photocatalytic tests for 1 h to establish adsorption-desorption equilibrium and illustrated in Fig. 10a. As it is depicted, NiO has adsorbed 100% of 20 ppm AO7 during an hour. Pure BiOI has adsorbed 71% of dye. As depicted, incorporating NiO to BiOI decreased adsorption capacity of composite compared with pure NiO or BiOI. In addition by increasing NiO content the amount of adsorbed AO7 is increased.

The photocatalytic activity of synthesized samples is investigated by degradation of AO7 under visible light illumination

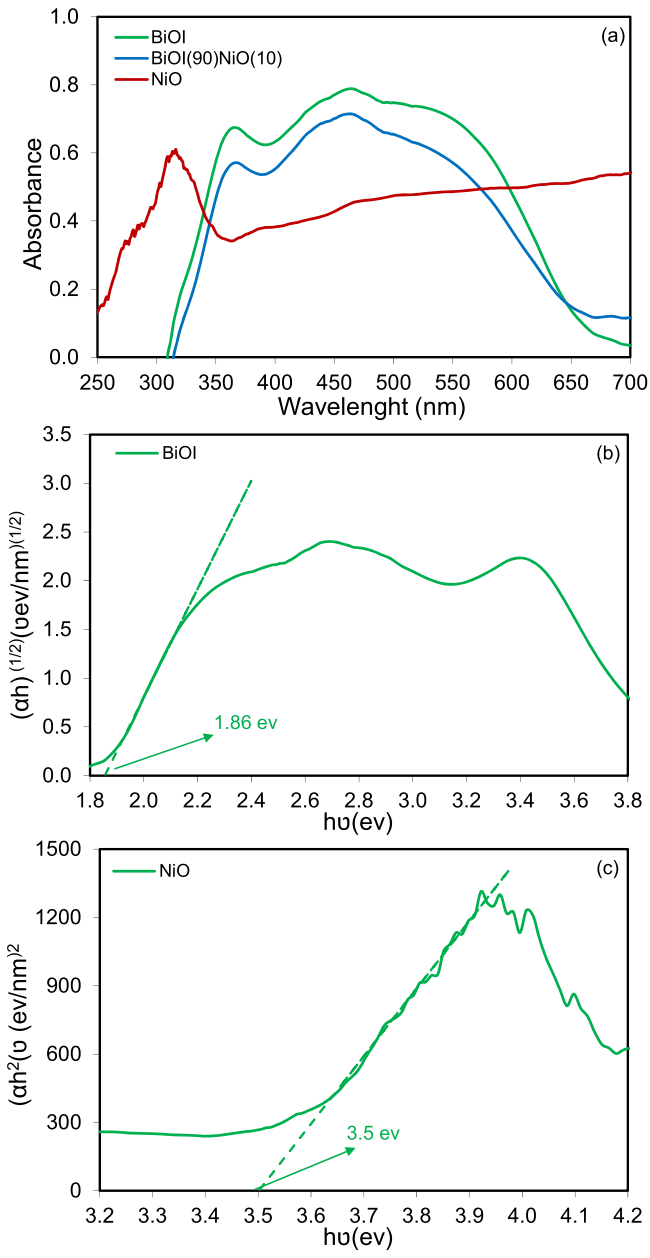

Fig. 8. (a) UV-vis diffuse reflectance spectra for BiOI, BiOI(90)-NiO(10) and NiO, (b) plot of (αhυ) 1/2 versus photon energy (hυ) for BiOI and (c) plot of (αhυ)2 versus photon energy(hυ) for NiO.

and the results are shown in Fig. 10b. AO7 is chemically stable and difficult to be decomposed, which shows a maximum absorption peak at 485 nm. As depicted in Fig. 10 when the catalyst is used to system after 180 min irradiation 69.3%, 97.5%, 79.4%,75.3% and 47.5% is photodegraded by BiOI, BiOI(90)/NiO(10), BiOI(80)/NiO(20), BiOI(60)/NiO(40) and BiOI(40)/NiO(60), respectively. As can be seen photodegradation of AO7 in the presence of pure NiO was almost negligible and this mainly resulted due to wide band gap of NiO which can exclusively respond to ultraviolet spectrum or fast recombination rate of charge carriers. The result stated clearly that NiO dramatically improved the photocatalytic activity of BiOI(90)/NiO(10) composite. A general look over reactor result shows that by increasing NiO content up to 40% the photoactivity of BiOI/NiO composite increased in comparison to pure NiO or BiOI, but further increment causes decrement in photocatalytic performance. The reason was considered to be that the p-p junction could

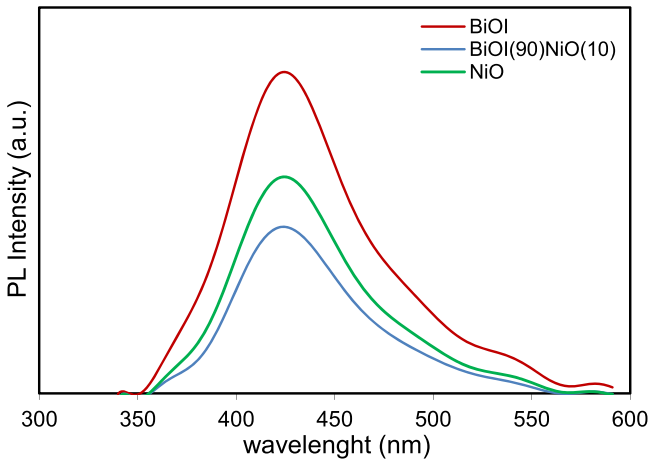

Fig. 9. Photoluminescence (PL) spectra of BiOI, p-BiOI(90)/p-NiO(10) and NiO at the excitation wavelength number of 320 nm.

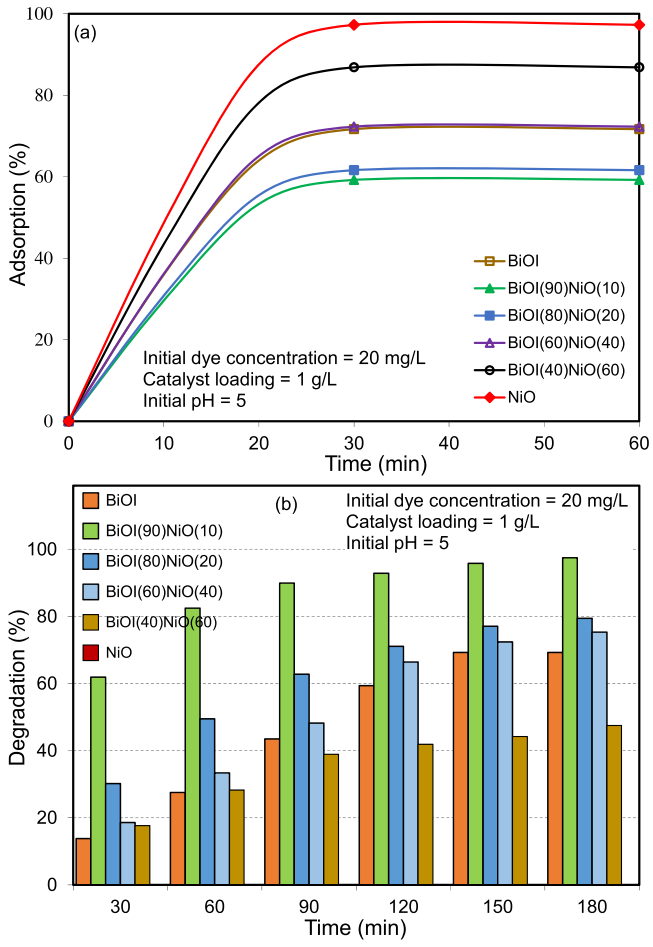

Fig. 10. (a) Adsorption experiment at dark before irradiation (b) Degradation performance of BiOI(x)-NiO(100-x) nanophotocatalysts toward water treatment under visible light.

not take a good role when there were so many NiO nanoparticles covering on the surface of BiOI and the light was difficult to reach the interface of the composites. As shown, among synthesized composite BiOI(90)/NiO(10) possess highest quantum efficiency. This is strongly explained by suitable heterojunction formation. This p-p type heterojunction between BiOI and NiO inhibits recombination

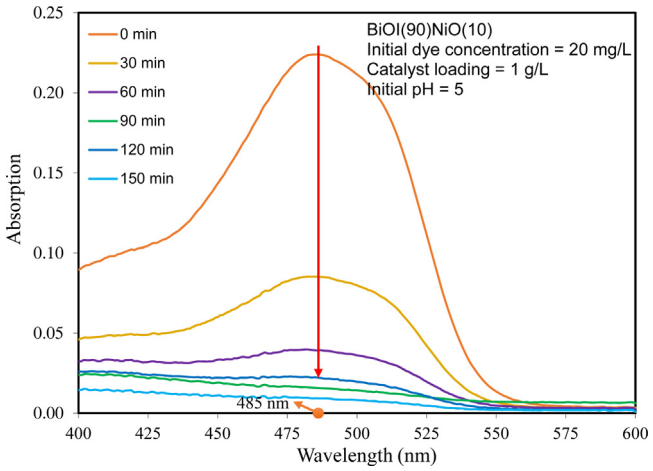

Fig. 11. Temporal evolution of spectral variations of AO7 degradation by p-BiOI(90)/p-NiO(10) composite for various times at 400–600 nm.

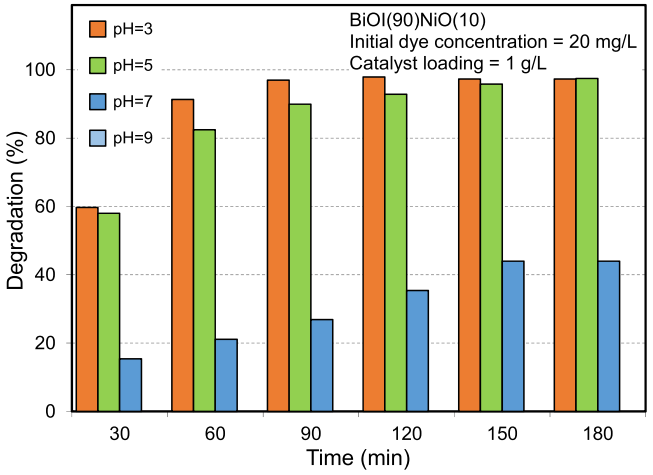

Fig. 12. Influence of pH on the performance of BiOI(x)-NiO(100-x) nanophotocatalysts toward water treatment.

of BiOI photo-excited electron-hole pairs in the presence of NiO nanoparticles.

3.2.2. *Temporal UV–vis absorption spectra of AO7 elimination*

Fig. 11 illustrates temporal evolution of spectral variations of AO7 degradation by BiOI(90)/NiO(10) composite for given durations. With increasing time the adsorption peak intensity diminishes gradually. However, sharp decrease is clearly observable at first half hour of irradiation. The main adsorption peak of AO7 located at 485 nm thoroughly vanished after 3 h illumination under visible light. In addition no new absorption bands were observed in visible light region, which confirms complete degradation of AO7 without any intermediates.

3.2.3. *Effect of pH*

It is accepted that pH of an initial dye solution exerts profound influence on photocatalytic performance. To this aim the effect of initial pH has been investigated and results were shown in Fig. 12. The results represent the degradation efficiency as a function of irradiation time. The initial pH was adjusted by sulfuric acid and ammonia aqueous solution. The pH experiments were done at four pH values of 3, 5, 7 and 9. The pH 3 was found to be the optimum pH. The photo-degradation efficiency greatly increases at low pH media. Vice versa the photoactivity is dissipated suddenly at higher pH values. It is concluded that acidic media is highly favored

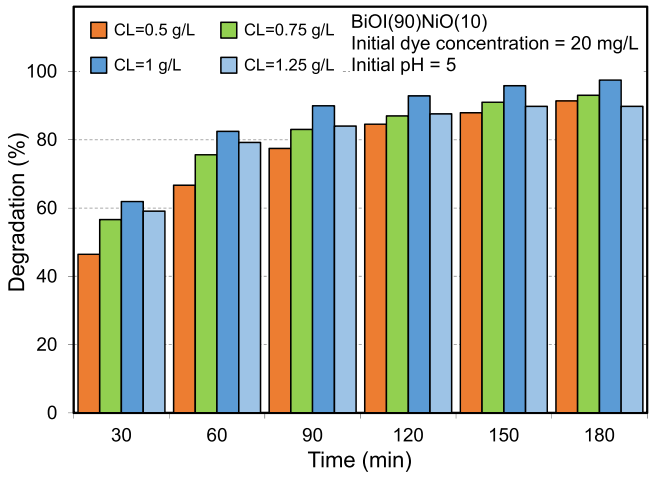

Fig. 13. Influence of catalyst loading on the performance of BiOI(x)-NiO(100-x) nanophotocatalysts toward water treatment.

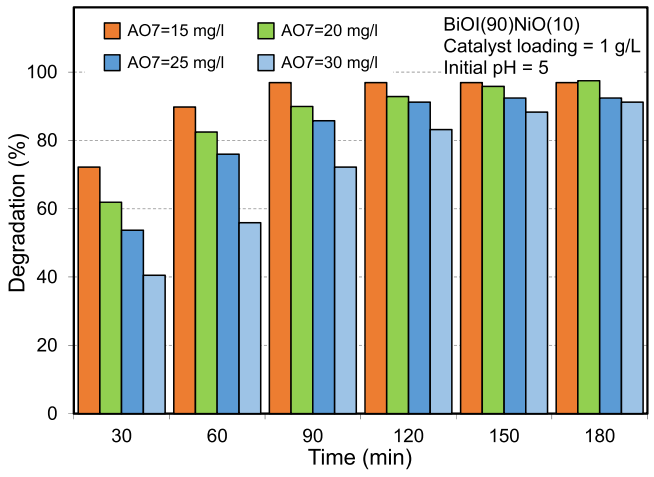

Fig. 14. Influence of acid orange concentration on the performance of BiOI(x)-NiO(100-x) nanophotocatalysts toward water treatment. (For interpretation of the references to colour in this figure legend, the reader is referred to the web version of this article.)

photodegradation process for BiOI(90)/NiO(10) in comparison with neutral or basic conditions. The pH mainly influences the surface charge properties of nanophotocatalyst. Surface charge is dependent on pH_{pzc} of nanophotocatalyst. At pH values lower than pH_{pzc} surface of photocatalyst is charged positively and at higher values negatively. According to several studies BiOI has acidic pH_{pzc} around 2 or 3 [68,69]. In this case due to anionic nature of AO7, acidic media contributes its adsorption owing to positive charge of nanophotocatalyst surface. However other unknown parameters may influence adsorption behavior of nanophotocatalyst.

3.2.4. Effect of photocatalyst loading

The effect of catalyst dosage on the photocatalytic degradation of AO7 is depicted in Fig. 13. As shown, the photocatalytic degradation of AO7 was found to be 93.2, 93.0, 97.5 and 89.8% at photocatalyst dosages of 0.5, 0.75, 1.0 and 1.25 g/L respectively, during 180 min. The photocatalytic activity of BiOI(90)/NiO(10) increased up to 1 g/L loading in the dye solution under visible light, but at 1.25 g/L the photoactivity decreased. This phenomenon can be explained by the following reasons: (i) light screening effect, (ii) nanophotocatalyst agglomeration, (iii) incident photon to electron conversion inefficiency due to low photon flux transmittance in the slurry.

3.2.5. Effect of acid orange concentration

The photocatalytic decolourization of acid orange 7 was investigated by varying the initial concentration of the dye for 15, 20, 25 and 30 ppm. The outcomes are illustrated in Fig. 14. The photocatalytic efficiency of BiOI/NiO(90/10) decreased while the acid orange 7 concentration increased. The quantum efficiency is dwindled due to the fact that high dye concentration limits the light accessibility to catalyst. Moreover illuminated photons are adsorbed by the excess dye in the slurry, which limits light accessibility for the surface of photocatalysts. Therefore, excited electron-hole pairs decreases. The degradation values of AO7 after irradiating 3 h under visible light were about 96.9, 97.5, 92.4 and 90% for 15, 20, 25 and 30 ppm AO7 dyes, respectively.

3.2.6. Reusability of photocatalyst

The reusability of photocatalyst is a deciding factor for practical applications. To examine the stability of BiOI(90)/NiO(10) photocatalyst, the sample in degradation of AO7 was tested in consecutive cycles under the same conditions and the experiment results are shown in Fig. 15. The degradation in the final 4th run was 93.1%. It implies that BiOI/NiO microflowers could be used as one of reusable and active nanophotocatalyst in environmental applications. In addition, results indicate that it does not photocorrode during photooxidation of AO7. Slight reduction in subsequent cycles may be due to catalyst loss and adsorption of dye or other intermediates.

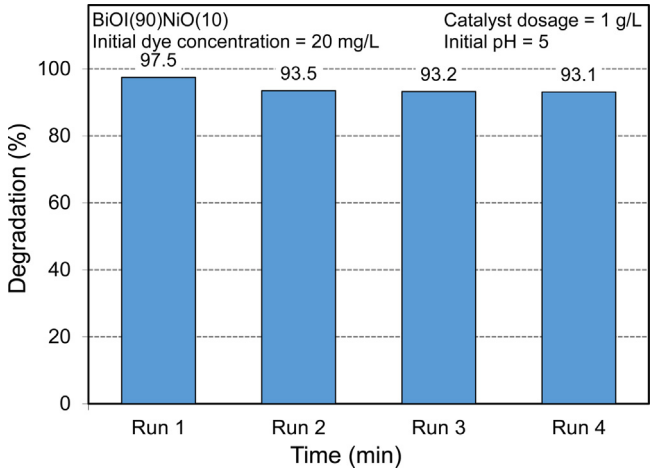

Fig. 15. Reusability test of p-BiOI(90)/p-NiO(10) heterostructure for degradation of AO7 under visible light irradiation (λ > 400).

3.3. Reaction mechanism of acid orange degradation

To obtain better understanding on the BiOI/NiO heterostructures and their enhanced visible light photocatalytic mechanism, the valence band (VB) and conduction band

(CB) edge potential were estimated via Mulliken electronegativity theory:

$$E_{vb} = X - E_0 + 0.5E_g \quad (3)$$

$$E_{cb} = E_{vb} - E_g \quad (4)$$

where E_{VB} is the VB edge potential, X is the absolute electronegativity of the semiconductor, which was the geometric mean of the electronegativity of the constituent atoms, E_0 is the standard electrode potential on the hydrogen scale (4.5 eV), and E_g is the band gap energy of the semiconductor. The Evb of NiO and BiOI are estimated to be 3.01and 2.63 eV respectively and Ecb evaluated to be −0.49 and 0.77 eV, respectively. It is well known that photocatalyst

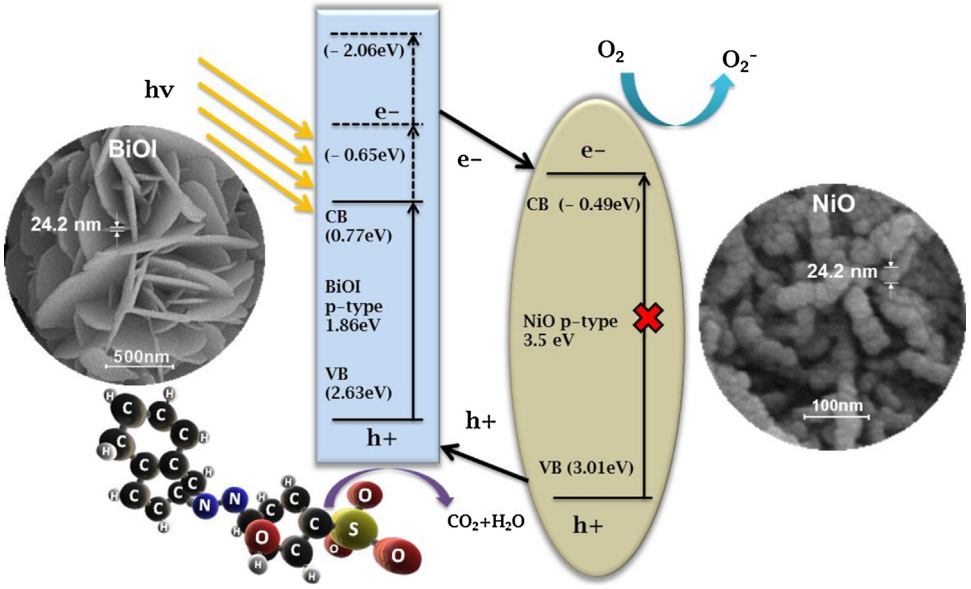

Fig. 16. Reaction mechanism for the removal of acid orange from water over BiOI(x)-NiO(100-x) nanophotocatalyst. (For interpretation of the references to colour in this figure legend, the reader is referred to the web version of this article.)

with more positive VB edge potentials exhibits stronger oxidative ability, so this could explain the higher visible light photocatalytic performance of BiOI/NiO nanophotocatalyst. On the other hand, it is highly accepted that better performance of heterostructures mainly depends on band gap structure, tight coupling and suitable heterojunction construction alignment. Fig. 16 is proposed to show detailed possible charge separation processes between NiO and BiOI. As depicted, when the BiOI/NiO composite was exposed to visible light, only BiOI can be excited due to its narrow band gap (1.86 eV). According to some reported results the electrons in the VB of BiOI can be excited to upper potential edge (-0.65 eV) with energy below than 2.95 eV ($\lambda > 420$ nm) because of its very narrow band gap [70–72]. In addition it is believed that by another mechanism, electrons in the VB of BiOI can also excited to higher position of −2.06 eV under visible light with energy less than 3.10 eV ($\lambda > 400$ nm) accordingly [73]. Thus the new reformed CB edge potentials of BiOI (−0.65 eV or −2.06) are more negative than that of NiO (−0.49 eV). The new proposed staggered alignments between BiOI and NiO are efficient architecture for enhancement of photocatalytic performance. Thus photo-induced electrons on the surface of BiOI can migrate to the CB of NiO through the interface. Therefore BiOI/NiO composite effectively alleviates the recombination of photogenerated electrons-hole pairs. As a consequence, augments the photocatalytic decolorization efficiency. Therefore, the improved photocatalytic activity under visible light irradiation for 3D BiOI/NiO hierarchical microflowers is ascribed to the efficient separation of photogenerated carriers. Consequently electrons accumulated on the CB of NiO reduce the dissolved O_2 to O_2^- due to the more negative CB edge potential than E_0 ($O_2/O_2^{\cdot -}$) (0.13 eV NHE) [42,71]. The O_2^- oxidants degrades AO7 to H_2O and CO_2 as final products. Photo-induced electrons after migration to CB of NiO, leave holes behind on the valence band of BiOI. As seen all of valence band position of samples are more positive than $^{\bullet}OH/OH^-$(1.99 eV), H_2O_2 (1.77 eV), and O_3 (2.07 eV) [73,74] indicating that photogenerated holes of such catalyst have strong oxidation ability than $OH^{\bullet}$ and H_2O_2. Therefore accumulated photo induced holes on the VB of BiOI directly oxidize AO7 to CO_2 and H_2O. It is evident that improved photoactivity of nanophotocatalyst involving BiOI and NiO attributed to the synergistic effect of p-p junction with staggered alignments. According to above statements, it is not surprising, that BiOI/NiO p-p heterostructures leads to much higher photoactivity than pure BiOI or NiO.

4. Conclusions

We have successfully constructed a novel flower-like BiOI/NiO nanocomposite by a simple solvothermal-precipitation method. Under visible light, BiOI(90)/NiO(10) composite exhibited excellent photocatalytic performance for AO7 degradation in comparison with the pure NiO, BiOI and BiOI(x)/NiO(100-x) heterojunctions. The morphological and optical studies revealed that the activity enhancement of BiOI/NiO attributed to efficient separation of photoinduced electrons and holes caused by heterostructure. Furthermore the results showed that the composite is highly active in acidic environment and the catalyst dosage has an optimum amount. In addition the effect of dye concentration has been investigated.

Acknowledgements

The authors gratefully acknowledge Sahand University of Technology for the financial support of the research as well as Iran Nanotechnology Initiative Council for complementary financial supports.

References

[1] S. Ahmed, M.G. Rasul, R. Brown, M.A. Hashib, Influence of parameters on the heterogeneous photocatalytic degradation of pesticides and phenolic contaminants in wastewater: a short review, J. Environ. Manage. 92 (2011) 311–330.
[2] M.N. Antipina, G.B. Sukhorukov, Remote control over guidance and release properties of composite polyelectrolyte based capsules, Adv. Drug Deliv. Rev. 63 (2011) 716–729.
[3] M. Moradi, M. Haghighi, S. Allahyari, Precipitation dispersion of Ag-ZnO nanocatalyst over functionalized multiwall carbon nanotube used in degradation of acid orange from wastewater, Process Saf. Environ. Prot. 107 (2017) 414–427.
[4] C.G. Anchieta, D. Sallet, E.L. Foletto, S.S. da Silva, O. Chiavone-Filho, C.A.O. do Nascimento, Synthesis of ternary zinc spinel oxides and their application in the photodegradation of organic pollutant, Ceram. Int. 40 (2014) 4173–4178.
[5] C.G. Anchieta, E.C. Severo, C. Rigo, M.A. Mazutti, R.C. Kuhn, E.I. Muller, E.M.M. Flores, R.F.P.M. Moreira, E.L. Foletto, Rapid and facile preparation of zinc ferrite (ZnFe2O4) oxide by microwave-solvothermal technique and its

catalytic activity in heterogeneous photo-Fenton reaction, Mater. Chem. Phys. 160 (2015) 141–147.
[6] Y. Ao, L. Xu, P. Wang, C. Wang, J. Hou, J. Qian, Y. Li, Graphene and TiO2 co-modified flower-like Bi2O2CO3: A novel multi-heterojunction photocatalyst with enhanced photocatalytic activity, Appl. Surf. Sci. 355 (2015) 411–418.
[7] Y. Bai, L. Ye, L. Wang, X. Shi, P. Wang, W. Bai, P.K. Wong, g-C3N4/Bi4O5I2 heterojunction with I3-/I- redox mediator for enhanced photocatalytic CO2 conversion, Appl. Catal. B: Environ. 194 (2016) 98–104.
[8] M.S. Ghodrati, M. Haghighi, J.S. Soltan Mohammadzadeh, B. Pourabas, E. Pipelzadeh, Phenol decomposition under sunlight using a sonochemically synthesized CdSe/TiO2 nanocatalyst, reaction kinetics, Mech. Catal. 104 (2011) 49–60.
[9] S. Bhukal, R. Sharma, S. Mor, S. Singhal, Mg-Co-Zn magnetic nanoferrites: characterization and their use for remediation of textile wastewater, Superlattices Microstruct. 77 (2015) 134–151.
[10] A.I. Borhan, P. Samoila, V. Hulea, A.R. Iordan, M.N. Palamaru, Photocatalytic activity of spinel ZnFe2-xCrxO4 nanoparticles on removal Orange I azo dye from aqueous solution, J. Taiwan Inst. Chem. Eng. 45 (2014) 1655–1660.
[11] J. Bai, Synthesis and photocatalytic activity of cobalt oxide doped ZnFe2O4-Fe2O3-ZnO mixed oxides, Mater. Lett. 63 (2009) 1485–1488.
[12] S. Matloubi Aghdam, M. Haghighi, S. Allahyari, L. Yosefi, Precipitation dispersion of various ratios of BiOI/BiOCl nanocomposite over g-C3N4 for promoted visible light nanophotocatalyst used in removal of acid orange 7 from water, J. Photochem. Photobiol. A: Chem. 338 (2017) 201–212.
[13] P. Margan, M. Haghighi, Microwave-Assisted hydrothermal synthesis of N-TiO2 nanophotocatalyst used in removal of acid orange 7 from wastewater, Nanoscale 3 (2017) 195–204.
[14] N. Asgari, M. Haghighi, S. Shafiei, Synthesis and physicochemical characterization of nanostructured Pd/Ceria-Clinoptilolite catalyst used for P-Xylene abatement from waste gas streams at low temperature, J. Chem. Technol. Biotechnol. 88 (2013) 690–703.
[15] J. Baneshi, M. Haghighi, N. Jodeiri, M. Abdollahifar, H. Ajamein, Homogeneous precipitation synthesis of cuO-ZrO2-CeO2-Al2O3 nanocatalyst used in hydrogen production via methanol steam reforming for fuel cell applications, Energy Convers. Manage. 87 (2014) 928–937.
[16] M. Maleki, M. Haghighi, Sono-Dispersion of cuS-CdS over TiO2 in one-Pot hydrothermal reactor as visible-Light-Driven nanostructured photocatalyst, J. Mol. Catal. A: Chem. 424 (2016) 283–296.
[17] J. Cao, X. Li, H. Lin, S. Chen, X. Fu, In situ preparation of novel p-n junction photocatalyst BiOI/(BiO)2CO3 with enhanced visible light photocatalytic activity, J. Hazard. Mater. 239-240 (2012) 316–324.
[18] J. Cao, X. Li, H. Lin, B. Xu, S. Chen, Q. Guan, Surface acid etching of (BiO)2CO3 to construct (BiO)2CO3/BiOX (X = Cl, Br I) heterostructure for methyl orange removal under visible light, Appl. Surf. Sci. 266 (2013) 294–299.
[19] J. Cao, C. Zhou, H. Lin, B. Xu, S. Chen, Surface modification of m-BiVO4 with wide band-gap semiconductor BiOCl to largely improve the visible light induced photocatalytic activity, Appl. Surf. Sci. 284 (2013) 263–269.
[20] L. Chen, R. Huang, M. Xiong, Q. Yuan, J. He, J. Jia, M.-Y. Yao, S.-L. Luo, C.-T. Au, S.-F. Yin, Room-Temperature synthesis of flower-Like BiOX (XCl, Br I) hierarchical structures and their visible-Light photocatalytic activity, Inorg. Chem. 52 (2013) 11118–11125.
[21] Q.W. Cao, X. Cui, Y.F. Zheng, X.C. Song, A novel CdWO4/BiOBr p-n heterojunction as visible light photocatalyst, J. Alloys Compd. 670 (2016) 12–17.
[22] C. Chang, L. Zhu, Y. Fu, X. Chu, Highly active Bi/BiOI composite synthesized by one-step reaction and its capacity to degrade bisphenol A under simulated solar light irradiation, Chem. Eng. J. 233 (2013) 305–314.
[23] F. Chen, C. Niu, Q. Yang, X. Li, G. Zeng, Facile synthesis of visible-light-active BiOI modified Bi2MoO6 photocatalysts with highly enhanced photocatalytic activity, Ceram. Int. 42 (2016) 2515–2525.
[24] P. Margan, M. Haghighi, Hydrothermal-Assisted Sol–Gel synthesis of Cd-Doped TiO2 nanophotocatalyst for removal of acid orange from wastewater, J. Sol-Gel Sci. Technol. 81 (2017) 556–569.
[25] Y.I. Choi, K.H. Jeon, H.S. Kim, J.H. Lee, S.J. Park, J.E. Roh, M.M. Khan, Y. Sohn, TiO2/BiOX (X = Cl, Br I) hybrid microspheres for artificial waste water and real sample treatment under visible light irradiation, Sep. Purif. Technol. 160 (2016) 28–42.
[26] Z. Cui, M. Si, Z. Zheng, L. Mi, W. Fa, H. Jia, Preparation and characterization of Ag3PO4/BiOI composites with enhanced visible light driven photocatalytic performance, Catal. Commun. 42 (2013) 121–124.
[27] L. Chen, S.-F. Yin, S.-L. Luo, R. Huang, Q. Zhang, T. Hong, P.C.T. Au, Bi2O2CO3/BiOI photocatalysts with heterojunctions highly efficient for visible-Light treatment of dye-Containing wastewater, Ind. Eng. Chem. Res. 51 (2012) 6760–6768.
[28] F. Duo, C. Fan, Y. Wang, Y. Cao, X. Zhang, One-pot hydrothermal synthesis of a novel BiPO4/BiOBr composite with enhanced visible light photocatalytic activities, Mater. Sci. Semicond. Process. 38 (2015) 157–164.
[29] W.J. Kim, D. Pradhan, B.-K. Min, Y. Sohn, Adsorption/photocatalytic activity and fundamental natures of BiOCl and BiOClxI1-x prepared in water and ethylene glycol environments, and Ag and Au-doping effects, Appl. Catal. B: Environ. 147 (2014) 711–725.
[30] E. Aghaei, M. Haghighi, Effect of crystallization time on properties and catalytic performance of nanostructured SAPO-34 molecular sieve synthesized at high temperatures for conversion of methanol to light olefins, Powder Technol. 269 (2015) 358–370.
[31] S. Aghamohammadi, M. Haghighi, S. Karimipour, A comparative synthesis and physicochemical characterizations of Ni/Al2O3-MgO nanocatalyst via sequential impregnation and sol-gel methods used for CO2 reforming of methane, J. Nanosci. Nanotechnol. 13 (2013) 4872–4882.
[32] Z. Hosseini, N. Taghavinia, N. Sharifi, M. Chavoshi, M. Rahman, Fabrication of high conductivity TiO2/Ag fibrous electrode by the electrophoretic deposition method, J. Phys. Chem. C 112 (2008) 18686–18689.
[33] P. Margan, M. Haghighi, Hydrothermal-assisted sol-gel synthesis of Cd-doped TiO2 nanophotocatalyst for removal of acid orange from wastewater, J. Sol-Gel Sci. Technol. (2016) 1–14.
[34] B. Palanisamy, C.M. Babu, B. Sundaravel, S. Anandan, V. Murugesan, Sol-gel synthesis of mesoporous mixed Fe2O3/TiO2 photocatalyst: application for degradation of 4-chlorophenol, J. Hazard. Mater. 252-253 (2013) 233–242.
[35] H. Huang, K. Xiao, K.Y. Liu, Y. Shixin Zhang, In situ composition-Transforming fabrication of BiOI/BiOIO3 heterostructure: semiconductor p-n junction and dominantly exposed reactive facets, Cryst. Growth Des. 16 (2016) 221–228.
[36] L. -w. Shan, G. -l. Wang, L. -z. Liu, Z. Wu, Band alignment and enhanced photocatalytic activation for α-Bi2O3/BiOCl (0 1) core-shell heterojunction, J. Mol. Catal. A: Chem. 406 (2015) 145–151.
[37] C. Tang, E. Liu, J. Fan, X. Hu, L. Kang, J. Wan, Heterostructured Ag3PO4/TiO2 nano-sheet film with high efficiency for photodegradation of methylene blue, Ceram. Int. 40 (2014) 15447–15453.
[38] Q. Wang, X. Shi, E. Liu, J.C. Crittenden, X. Ma, Y. Zhang, Y. Cong, Facile synthesis of AgI/BiOI-Bi2O3 multi-heterojunctions with high visible light activity for Cr(VI) reduction, J. Hazard. Mater. 317 (2016) 8–16.
[39] C.-Z. Zheng, C.-Y. Zhang, G.-H. Zhang, D.-J. Zhao, Y.-Z. Wang, Enhanced photocatalytic performance of g-C3N4 with BiOCl quantum dots modification, Mater. Res. Bull. 55 (2014) 212–215.
[40] Y. Zhu, Y. Wang, Q. Ling, Y. Zhu, Enhancement of full-spectrum photocatalytic activity over BiPO4/Bi2WO6 composites, Appl. Catal. B: Environ. 200 (2017) 222–229.
[41] Z. Zhu, Y. Yan, J. Li, Preparation of flower-like BiOBr-WO3-Bi2WO6 ternary hybrid with enhanced visible-light photocatalytic activity, J. Alloys Compd. 651 (2015) 184–192.
[42] H. Li, Z. Jin, H. Sun, L. Sun, Q. Li, X. Zhao, C.-J. Jia, W. Fan, Facile fabrication of p-BiOI/n-Zn2SnO4 heterostructures with highly enhanced visible light photocatalytic performances, Mater. Res. Bull. 55 (2014) 196–204.
[43] H. Li, Y. Cui, W. Hong, High photocatalytic performance of BiOI/Bi2WO6 toward toluene and Reactive Brilliant Red, Appl. Surf. Sci. 264 (2013) 581–588.
[44] C. Liao, Z. Ma, G. Dong, J. Qiu, BiOI nanosheets decorated TiO2 nanofiber: tailoring water purification performance of photocatalyst in structural and photo-responsivity aspects, Appl. Surf. Sci. 314 (2014) 481–489.
[45] S. Han, J. Li, K. Yang, J. Lin, Fabrication of a β-Bi2O3/BiOI heterojunction and its efficient photocatalysis for organic dye removal, Chin. J. Catal. 36 (2015) 2119–2126.
[46] R. Khoshbin, M. Haghighi, N. Asgari, Direct synthesis of dimethyl ether on the admixed nanocatalystsof CuO-ZnO-Al2 O3 and HNO3-modified clinoptilolite at high pressures: surface properties and catalytic performance, Mater. Res. Bull. 48 (2013) 767–777.
[47] P. Sadeghpour, M. Haghighi, Synthesis of nanostructured mnNiAPSO-34 catalyst: catalytic properties and performance, J. Adv. Mater. Process. 2 (2014) 49–66.
[48] S.M. Sajjadi, M. Haghighi, A.A. Eslami, F. Rahmani, Hydrogen production via CO2-reforming of methane over Cu and Co doped Ni/Al2O3 nanocatalyst: impregnation versus sol-gel method and effect of process conditions and promoter, J. Sol-Gel Sci. Technol. 67 (2013) 601–617.
[49] S.M. Sajjadi, M. Haghighi, F. Rahmani, Sol-gel synthesis and catalytic performance of Ni-Co/Al2O3-MgO-ZrO2 nanocatalyst with different ZrO2-loadings used in CH4/CO2 reforming for hydrogen production, Int. J. Oil Gas Coal Technol. 8 (2014) 304–324.
[50] L. Yosefi, M. Haghighi, S. Allahyari, S. Ashkriz, Effect of ultrasound irradiation and Ni-loading on properties and performance of CeO2-doped Ni/clinoptilolite nanocatalyst used in polluted air treatment, Process Saf. Environ. Prot. 95 (2015) 26–37.
[51] J. Wang, A. Han, S. Jaenicke, G.-K. Chuah, Chapter 6 – advances in sorbents and photocatalytic materials for water remediation, in: New and Future Developments in Catalysis, Elsevier, Amsterdam, 2013, pp. 127–153.
[52] Y. Ku, C.-N. Lin, W.-M. Hou, Characterization of coupled NiO/TiO2 photocatalyst for the photocatalytic reduction of Cr(VI) in aqueous solution, J. Mol. Catal. A: Chem. 349 (2011) 20–27.
[53] Y. Jiao, Y. Liu, B. Yin, S. Zhang, F. Qu, X. Wu, Hybrid α-Fe2O3@NiO heterostructures for flexible and high performance supercapacitor electrodes and visible light driven photocatalysts, Nano Energy 10 (2014) 90–98.
[54] R.K. Gupta, K. Ghosh, P.K. Kahol, Fabrication and characterization of NiO/ZnO p-n junctions by pulsed laser deposition, Phys. E Low-Dimension. Syst. Nanostruct. 41 (2009) 617–620.
[55] Z. Khan, M. Khannam, N. Vinothkumar, M. De, M. Qureshi, Hierarchical 3D NiO-CdS heteroarchitecture for efficient visible light photocatalytic hydrogen generation, J. Mater. Chem. 22 (2012) 12090–12095.
[56] H.-Y. Chen, L.-G. Qiu, J.-D. Xiao, S. Ye, X. Jiang, Y.-P. Yuan, Inorganic-organic hybrid NiO-g-C3N4 photocatalyst for efficient methylene blue degradation using visible light, RSC Adv. 4 (2014) 22491–22496.
[57] S.M. Sajjadi, M. Haghighi, F. Rahmani, Dry reforming of greenhouse gases CH4/CO2 over MgO-promoted Ni-Co/Al2O3-ZrO2 nanocatalyst: effect of MgO addition via sol-gel method on catalytic properties and hydrogen yield, J. Sol-Gel Sci. Technol. 70 (2014) 111–124.

[58] M. Sharifi, M. Haghighi, M. Abdollahifar, Hydrogen production via reforming of biogas over nanostructured Ni/Y catalyst: effect of ultrasound irradiation and Ni-content on catalyst properties and performance, Mater. Res. Bull. 60 (2014) 328–340.
[59] M. Sharifi, M. Haghighi, M. Abdollahifar, Sono-dispersion of bimetallic Ni-Co over zeolite Y used in conversion of greenhouse gases CH4/CO2 to high valued syngas, J. Nat. Gas Sci. Eng. 23 (2015) 547–558.
[60] Y. Vafaeian, M. Haghighi, S. Aghamohammadi, Ultrasound assisted dispersion of different amount of Ni over ZSM-5 used as nanostructured catalyst for hydrogen production via CO2 reforming of methane, Energy Convers. Manage. 76 (2013) 1093–1103.
[61] A. Talati, M. Haghighi, F. Rahmani, Impregnation vs. coprecipitation dispersion of Cr over TiO2 and ZrO2 used as active and stable nanocatalysts in oxidative dehydrogenation of ethane to ethylene by carbon dioxide, RSC Adv. 6 (2016) 44195–44204.
[62] L. Yosefi, M. Haghighi, S. Allahyari, S. Ashkriz, The beneficial use of HCl-activated natural zeolite in ultrasound assisted synthesis of Cu/clinoptilolite-CeO2 nanocatalyst used for catalytic oxidation of diluted toluene in air at low temperature, J. Chem. Technol. Biotechnol. 90 (2015) 765–774.
[63] L. Yosefi, M. Haghighi, S. Allahyari, R. Shokrani, S. Ashkriz, Abatement of toluene from polluted air over Mn/Clinoptilolite-CeO2 nanopowder: impregnation vs. ultrasound assisted synthesis with various Mn-loading, Adv. Powder Technol. 26 (2015) 602–611.
[64] Z. Liang, R. Huo, Y.-X. Yin, F. Zhang, S. Xu, Y.-G. Guo, Carbon-supported Ni@NiO/Al2O3 integrated nanocomposite derived from layered double hydroxide precursor as cycling-stable anode materials for lithium-ion batteries, Electrochim. Acta 108 (2013) 429–434.
[65] R.K. Sharma, R. Ghose, Synthesis of porous nanocrystalline NiO with hexagonal sheet-like morphology by homogeneous precipitation method, Superlattices Microstruct. 80 (2015) 169–180.
[66] J. Li, Y. Yu, L. Zhang, Bismuth oxyhalide nanomaterials: layered structures meet photocatalysis, Nanoscale 6 (2014) 8473–8488.
[67] L. Yosefi, M. Haghighi, S. Allahyari, Solvothermal synthesis of flowerlike p-BiOI/n-ZnFe2O4 with enhanced visible light driven nanophotocatalyst used in removal of acid orange 7 from wastewater, Sep. Purif. Technol. 178 (2017) 18–28.
[68] Y. Xiang, P. Ju, Y. Wang, Y. Sun, D. Zhang, J. Yu, Chemical etching preparation of the Bi2WO6/BiOI p–n heterojunction with enhanced photocatalytic antifouling activity under visible light irradiation, Chem. Eng. J. 288 (2016) 264–275.
[69] Z. K.-H. Ye, J. Chai, X. Gu, C. Yu, Y. Zhao, W. Mai Zhang, BiOI–BiVO4 photoanodes with significantly improved solar water splitting capability: p?n junction to expand solar adsorption range and facilitate charge carrier dynamics, Nano Energy 18 (2015) 222–231.
[70] J. Cao, B. Xu, B. Luo, H. Lin, S. Chen, Novel BiOI/BiOBr heterojunction photocatalysts with enhanced visible light photocatalytic properties, Catal. Commun. 13 (2011) 63–68.
[71] H. Lin, H. Ye, X. Li, J. Cao, S. Chen, Facile anion-exchange synthesis of BiOI/BiOBr composite with enhanced photoelectrochemical and photocatalytic properties, Ceram. Int. 40 (2014) 9743–9750.
[72] Z. Liu, H. Ran, B. Wu, P. Feng, Y. Zhu, Synthesis and characterization of BiOI/BiOBr heterostructure films with enhanced visible light photocatalytic activity, Coll. Surf. A 452 (2014) 109–114.
[73] X. Jia, J. Cao, H. Lin, Y. Chen, W. Fu, S. Chen, One-pot synthesis of novel flower-like BiOBr0.9I0.1/BiOI heterojunction with largely enhanced electron-hole separation efficiency and photocatalytic performances, J. Mol. Catal. A: Chem. 409 (2015) 94–101.
[74] H. Huang, K. Xiao, Y. He, T. Zhang, F. Dong, X. Du, Y. Zhang, In situ assembly of BiOI@Bi12O17Cl2 p-n junction: charge induced unique front-lateral surfaces coupling heterostructure with high exposure of BiOI {001} active facets for robust and nonselective photocatalysis, Appl. Catal. B: Environ. 199 (2016) 75–86.